RESEARCH ARTICLE | FEBRUARY 07 2024

Hybrid particle-spectral method for kinetic plasma simulations

Oleksandr Chapurin ; Oleksandr Koshkarov ; Gian Luca Delzanno ; Vadim Roytershteyn ; Peter Brady ; Robert Chiodi ; Cale Harnish ; Daniel Livescu

Phys. Plasmas 31, 023903 (2024)
https://doi.org/10.1063/5.0179464

Hybrid particle-spectral method for kinetic plasma simulations

Cite as: Phys. Plasmas **31**, 023903 (2024); doi: 10.1063/5.0179464
Submitted: 2 October 2023 · Accepted: 5 January 2024 ·
Published Online: 7 February 2024

Oleksandr Chapurin,[1,a] Oleksandr Koshkarov,[1,b] Gian Luca Delzanno,[1,c] Vadim Roytershteyn,[2,d] Peter Brady,[3,e] Robert Chiodi,[3,f] Cale Harnish,[3,g] and Daniel Livescu[3,h]

AFFILIATIONS

[1]T-5 Applied Mathematics and Plasma Physics Group, Los Alamos National Laboratory, Los Alamos, New Mexico 87545, USA
[2]Space Science Institute, Boulder, Colorado 80301, USA
[3]CCS-2 Computational Physics and Methods Group, Los Alamos National Laboratory, Los Alamos, New Mexico 87545, USA

[a]**Author to whom correspondence should be addressed:** chapurin@lanl.gov
[b]**Electronic mail:** koshkarov@lanl.gov
[c]**Electronic mail:** delzanno@lanl.gov
[d]**Electronic mail:** vroytershteyn@spacescience.org
[e]**Electronic mail:** ptb@lanl.gov
[f]**Electronic mail:** robertchiodi@lanl.gov
[g]**Electronic mail:** charnish@lanl.gov
[h]**Electronic mail:** livescu@lanl.gov

ABSTRACT

A hybrid model for numerical solutions of the Vlasov–Poisson equations is presented, which blends spectral and particle approaches. The model splits the distribution function for plasma species into both spectral and particle representations in the velocity space to combine the advantages of each approach. The spectral representation leverages asymmetrically weighted Hermite basis, whereas the particle representation leverages the particle-in-cell method. Configuration phase space is decomposed with the Fourier method, which is well suited for periodic problems. We derive conservation equations for mass, momentum, and energy for the proposed combined method. It is shown that the coupling error between the two methods is absent in the semi-discrete setting (not taking into account time discretization). Finally, numerical test cases are presented simulating a weak electron beam interaction with plasma, leading to beam–plasma instability. The initially localized electron beam evolved into a highly non-equilibrium distribution function in the velocity space. A small growth rate and the resonance nature of instability make it difficult to obtain accurate solutions for purely particle methods due to noise, which falls as $\sim 1/\sqrt{N_p}$ with a number of particles. At the same time, purely spectral methods may require a large number of modes to capture the highly non-equilibrium state of the evolved beam. We show that the hybrid method is well suited for such problems: it reproduces the linear stage as well as nonlinear dynamics with sufficient accuracy using a highly non-equilibrium distribution function.

I. INTRODUCTION

Accurate numerical solutions of the nonlinear Vlasov–Maxwell (VM) equations are of great interest in many situations. For example, describing mechanisms of energy release,[1,2] plasma turbulence,[3] and particle acceleration.[4] However, such solutions present considerable challenges. First, the particle distribution function (PDF) evolves in six-dimensional phase space and this high dimensionality greatly increases the number of unknowns. Second, plasmas are characterized by several disparate internal scales (e.g., Debye length, Larmor radii, inertial lengths, etc.), which need to be simultaneously resolved but that are normally orders-of-magnitude smaller than the system size. For example, global simulations of the solar wind interaction with the Earth's magnetosphere involve system sizes of the order of hundreds of Earth radii ($\sim 10^6$ km) but may need to resolve narrow boundary layers of width 1 km, while local Debye lengths in the inner magnetosphere range between 1 and 100 m. Additionally, magnetized plasmas can be strongly anisotropic, with characteristic spatial and temporal scales different by several orders of magnitude along and across the magnetic field.

There exist various numerical methods for the solution of the VM system. One can classify them by the phase space discretization.

The most popular technique is the particle-in-cell (PIC) method.[5] In the PIC method, the phase space is discretized with macro-particles, which follow the characteristics of the Vlasov equation. Such discretization results in a very efficient but relatively low accuracy method. Thus, while an important strength of a particle approach is its ability to resolve complex PDFs, the poor scaling of the statistical sampling noise with the number of macro-particles N_p, which falls as $\sim 1/\sqrt{N_p}$, is a major limitation. Another approach is based on a spectral discretization of velocity space,[6–12] where the PDF is expanded in a series of basis functions similar to the classic moment expansion. These methods do not suffer from statistical noise but convergence of the expansion could be slow and positivity of the PDF is not guaranteed. The proper choice of basis functions (i.e., its optimization)[13–15] can dramatically improve convergence, making it much more computationally efficient/accurate than PIC methods in some situations.[16] A third class of methods, the so-called Eulerian–Vlasov methods,[17–22] discretize phase space with a six-dimensional mesh.

In this paper, we introduce a hybrid method that combines PIC and spectral approaches in order to exploit the advantages offered by both methods. Conceptually, we divide the PDF into distinct parts that are separately represented with either PIC macro-particles or by a spectral expansion. The distinct parts of the PDF are evolved according to their own Vlasov equation, coupled by the self-consistent electromagnetic field, which combines the contributions of all parts. The need for PDF separation may depend on the specific problem at hand, but the general idea is to treat the bulk part of the PDF with a suitable spectral expansion and treat the remaining part of the PDF, which can show more complex structures (e.g., shocks, beams, etc.), with macro-particles. In this work, the main focus is on velocity space discretizations. The spatial coordinate is expanded in Fourier space, which is well suited for periodic domain problems. We analyze the conservation properties of the proposed method in a semi-discrete setting (assuming the temporal variable is continuous) and show the absence of a coupling error between the two representations for mass, momentum, and energy conservation. Thus, the conservation properties of the hybrid method are inherited from both the PIC and spectral approaches. The present implementation exploits the cloud-in-cell method (linear interpolation for the shape function)[23] for the PIC approach, which conserves total mass and momentum. The asymmetric Hermite polynomial basis is used for the spectral approach, which conserves total mass, momentum, and energy[13] (note that a fully implicit time integration scheme is required for energy conservation[9]).

We discuss a particular implementation of this general concept to the one-dimensional electrostatic VM system and apply it to simulations of the interaction between a tenuous electron beam and a background plasma, i.e., by solving the Vlasov–Poisson system. In this problem, the denser background (bulk) plasma is represented with a spectral expansion, while the beam is represented using macro-particles. Two cases are considered: one is a short-box problem where only one linearly unstable mode is resolved, and another is a larger system size with more complex nonlinear dynamics. In the first case, we compare the hybrid model to a fully spectral (reference) solution and show the expected statistical convergence of the hybrid method with the number of particles. In the second case, we demonstrate the capabilities of the hybrid method resolving a distribution function, which significantly deviates from a Maxwellian distribution resulting from the beam–plasma interaction. For this case, we show that the linear growth rates are in agreement with the kinetic dispersion equation for the unstable modes, which serve as an additional verification. For both numerical tests, we demonstrate the conservation properties of the hybrid method, which are consistent with our analysis.

The paper is organized as follows: Sec. II introduces the mathematical formulation of the new method on the Vlasov–Poisson system. Derivations of conservation properties of the new method are shown in Sec. III. The results comparing the new hybrid method against a fully spectral method are discussed in Sec. IV. Finally, Sec. V draws conclusions of the paper.

II. METHOD DESCRIPTION

We consider the one-dimensional Vlasov–Poisson system describing the behavior of a collisionless plasma in the electrostatic, unmagnetized limit. The Vlasov–Poisson system for the distribution function $f^\zeta(x, v, t)$ of each plasma species ζ (e.g., electrons and ions) and the electric field $E(x, t)$ takes the form

$$\frac{\partial f^\zeta}{\partial t} + v\frac{\partial f^\zeta}{\partial x} + \frac{q^\zeta}{m^\zeta}E\frac{\partial f^\zeta}{\partial v} = 0, \tag{1}$$

$$\frac{\partial E}{\partial x} = \sum_\zeta q^\zeta \int_{-\infty}^{+\infty} f^\zeta dv = \sum_\zeta \rho^\zeta, \tag{2}$$

where ρ^ζ is the charge density for species ζ. We consider the case of periodic boundary conditions

$$f^\zeta(t, 0, v) = f^\zeta(t, L, v), \quad E(t, 0) = E(t, L), \quad \lim_{v\to\pm\infty} f^\zeta(t, x, v) = 0, \tag{3}$$

where $t \geq 0$, $x \in [0, L]$, and $v \in \mathbb{R}$ are time, space, and velocity variables, respectively, L is the length of the spatial domain, and q^ζ and m^ζ are the charge and mass of species ζ, respectively. In Eqs. (1) and (2), all quantities are dimensionless with the normalization units defined as

$$t = t^d\omega_{pe}, \quad x = \frac{x^d}{\lambda_D}, \quad E = \frac{e\lambda_D}{T_e}E^d, \quad v = \frac{v^d}{v_{the}}, \tag{4}$$

$$f = v_{the}\frac{f^d}{n_0}, \quad q = \frac{q^d}{e}, \quad m = \frac{m^d}{m_e}, \tag{5}$$

where the superscript d denotes the dimensional variables; $\omega_{pe} = \sqrt{4\pi e^2 n_0/m_e}$ is the electron plasma frequency; $\lambda_D = \sqrt{T_e/4\pi e^2 n_0}$ is the electron Debye length; $v_{the} = \sqrt{T_e/m_e}$ is the electron thermal velocity; n_0 is the reference plasma density; e, m_e, and T_e are the scalar elementary charge, the electron mass, and the reference electron temperature, respectively.

We seek the distribution function of the form

$$f^\zeta = f^{s\zeta} + f^{p\zeta}, \tag{6}$$

where both $f^{s\zeta}$ and $f^{p\zeta}$ satisfy Vlasov's equation (1), but only f^ζ satisfies the full Vlasov–Poisson system (1–2) that involves all species ζ. The self-consistent electric field is provided by Eq. (2), which involves the full distribution function f^ζ.

The Vlasov equation for $f^{s\zeta}$, where the superscript "$s\zeta$" stands for *"spectral" species*, is solved numerically by using the spectral method developed in Refs. 8 and 9. The Vlasov equation for $f^{p\zeta}$, where superscript "$p\zeta$" stands for *"particle" species*, is numerically solved by using

the particle-in-cell (PIC) technique.[5] In general, one can have a variety of *spectral species* and *particle species*, i.e., Eq. (6) will take the form

$$f^{\zeta} = \sum_{s} f^{s_\zeta} + \sum_{p} f^{p_\zeta}, \tag{7}$$

and the decomposition can vary adaptively in time. For simplicity, in this work, the splitting adopted in Eq. (6) is defined only once at the beginning of the simulation. In some situations, dynamically transferring parts of f^{p_ζ} to f^{s_ζ} and vice versa would be advantageous, but this is left for future work.

A. Discretization of the Vlasov equation with the PIC technique

The distribution function f^{p_ζ} for each particle species is provided by using the explicit formulation of the PIC method.[5] In the PIC technique, the plasma is characterized by macro-particles, each representing a large number of particles of the physics system of interest that occupy a given region of phase space. The trajectories of the macro-particles, given by characteristics of the Vlasov equation, are

$$\frac{dx_i^{p_\zeta}}{dt} = v_i^{p_\zeta}, \quad \frac{dv_i^{p_\zeta}}{dt} = \frac{q^{p_\zeta}}{m^{p_\zeta}} E(x_i^{p_\zeta}), \tag{8}$$

for $i = 1, \ldots, N^{p_\zeta}$, where N^{p_ζ} is the number of macro-particles describing species p_ζ, $x_i^{p_\zeta}$, $v_i^{p_\zeta}$, q^{p_ζ}, and m^{p_ζ} are the position, velocity, charge, and mass of the ith macro-particle, respectively, and $E(x_i^{p_\zeta})$ is the electric field at the macro-particle position $x_i^{p_\zeta}$.

The electric field at the macro-particle position, $E(x_i^{p_\zeta})$, is computed by

$$E(x_i^{p_\zeta}) = \sum_{j=0}^{N_x-1} E_j S(x_j - x_i^{p_\zeta}), \tag{9}$$

where E_j is the electric field at the N_x nodes $x_j = jL/N_x = j\Delta x (j = 0, \ldots, N_x - 1)$ of a uniform Eulerian grid and $S(x - x_i^{p_\zeta})$ is the so-called shape function.[23] In the present paper, we use a linear interpolation for the shape function, corresponding to the cloud-in-cell algorithm.[23]

Similarly, the charge density on the grid, necessary for the solution of Poisson's equation (2), is obtained from the interpolation of the macro-particle's charge

$$\rho_j^{p_\zeta} = \rho^{p_\zeta}(x_j) = \frac{1}{\Delta x} \sum_{i=1}^{N_p^{p_\zeta}} q^{p_\zeta} w^{p_\zeta} S(x_j - x_i^{p_\zeta}), \tag{10}$$

where w^{p_ζ} is the weight of each macro-particle, and $N_p^{p_\zeta}$ is the number of particles of the corresponding particle species.

B. Discretization of the Vlasov equation with the spectral method

In order to solve Eq. (1) for the distribution function f^{s_ζ}, we consider the Galerkin method based on the Fourier trigonometric functions for the space representation[24] and the asymmetrically weighted Hermite (AWH) basis functions for the velocity representation.[6–9,13] Using Fourier trigonometric functions allows a very natural implementation of periodic boundary conditions in space. The Fourier trigonometric functions are defined by

$$\eta_k(x) = \exp\left(\frac{2\pi}{L} ikx\right), \tag{11}$$

and satisfy the orthogonality relation

$$\frac{1}{L}\int_0^L \eta_k(x)\eta_{-k'}(x)\, dx = \delta_{k,k'}. \tag{12}$$

The asymmetrically-weighted Hermite basis functions consist of two sets of functions

$$\Psi_n(\xi) = \frac{1}{\sqrt{\pi 2^n n!}} H_n(\xi) e^{-\xi^2}, \quad \Psi^n(\xi) = \frac{1}{\sqrt{2^n n!}} H_n(\xi), \tag{13}$$

where $H_n(\xi)$ is the Hermite polynomial of degree n given by the recursive definition

$$H_0(\xi) = 1, \quad H_1(\xi) = 2\xi, \quad H_{n+1}(\xi) = 2\xi H_n(\xi) - 2nH_{n-1}(\xi). \tag{14}$$

These two sets of functions satisfy the duality relation expressed by the orthogonality condition

$$\int_{-\infty}^{+\infty} \Psi_n(\xi)\Psi^m(\xi) d\xi = \delta_{n,m}. \tag{15}$$

Next, we expand the distribution function and the electric field as

$$f^{s_\zeta}(t, x, v) = \sum_{n=0}^{N_v-1} \sum_{k=-N_k}^{N_k} C_{n,k}^{s_\zeta}(t) \Psi_n(\xi^{s_\zeta}) \eta_k(x), \tag{16}$$

$$E(x) = \sum_{k=-N_k}^{N_k} \hat{E}_k \eta_k(x), \tag{17}$$

where N_v is the number of Hermite modes, N_k is the number of Fourier modes in space satisfying the condition $N_x = 2N_k + 1$, and $\xi^{s_\zeta} = (v - u^{s_\zeta})/\alpha^{s_\zeta}$ with u^{s_ζ} and α^{s_ζ} being the user-defined constant parameters. Substituting Eqs. (16) and (17) into Eq. (1) for f^{s_ζ} and using the orthogonality relations, we obtain the following system of equations:[16]

$$\frac{dC_{n,k}^{s_\zeta}}{dt} = \mathfrak{L}_{n,k}[C^{s_\zeta}] + \mathfrak{N}_{n,k}[C^{s_\zeta}] - \nu g(n) C_{n,k}^{s_\zeta}, \tag{18}$$

with indices $n = 0, \ldots, N_v - 1$ and $k = -N_k, \ldots, N_k$,

$$\mathfrak{L}_{n,k}[C^{s_\zeta}] = -\alpha^{s_\zeta} \frac{2\pi ik}{L} \left(\sqrt{\frac{n}{2}} C_{n-1,k}^{s_\zeta} + \frac{u^{s_\zeta}}{\alpha^{s_\zeta}} C_{n,k}^{s_\zeta} + \sqrt{\frac{n+1}{2}} C_{n+1,k}^{s_\zeta} \right), \tag{19}$$

$$\mathfrak{N}_{n,k}[C^{s_\zeta}] = \frac{q^{s_\zeta}}{m^{s_\zeta}\alpha^{s_\zeta}} \left[\hat{E}_* * \sqrt{2n} C_{n-1,*}^{s_\zeta} \right]_k, \tag{20}$$

and the convolution operator defined as

$$[A_* * B_*]_k = \sum_{k'=-N_k}^{N_k} A_{k-k'} B_{k'}, \tag{21}$$

where $*$ subscript indicates the index over which the convolution is performed. The last term in (18) is an artificial collision operator,

which is commonly introduced in spectral (and Eulerian–Vlasov) methods to prevent filamentation (i.e., recurrence), with the collisional rate ν. In this work, we used the collisional operator introduced in Ref. 16, in the form

$$g(n) = \frac{n(n-1)(n-2)}{(N_v-1)(N_v-2)(N_v-3)}, \tag{22}$$

which is designed to be nonzero for the higher moments, but not to change the coefficients $C^{s\zeta}_{n,k}$ for $n<3$. This choice avoids the error in mass, momentum, and energy conservation due to artificial collisionality.

The Fourier component of the spectral charge density $\hat{\rho}^{s\zeta}_k$ is obtained by analytically computing the integral on the right-hand side of (2) as follows:

$$\hat{\rho}^{s\zeta}_k = q^{s\zeta}\alpha^{s\zeta}C^{s\zeta}_{0,k}. \tag{23}$$

A straightforward implementation of the convolution (21) would be inefficient as the algorithmic complexity scales like $O(N_x^2)$. A more efficient implementation is possible in real space, where it has a local form,[25] using the fast Fourier transform (FFT) algorithm.[26] This reduces the algorithmic complexity to $O(N_x \log N_x)$. It is worth mentioning that in our work, we did not use any dealiasing technique as there were no obvious symptoms of aliasing errors (e.g., numerical instabilities, etc.[24]) that may be introduced in the numerical approximation of nonlinear terms by spectral methods.

C. Spectral discretization of Poisson's equation

In the hybrid method, the PIC and spectral parts are coupled by Poisson's equation (2). The Poisson equation is solved numerically by the Fourier-based spectral method, and its discrete formulation is obtained using the expansion (17) and the orthogonality condition (12)

$$\hat{E}_k = \frac{L}{2\pi i k}\left(\sum_\zeta \hat{\rho}^{s\zeta}_k + \sum_\zeta \hat{\rho}^{p\zeta}_k\right), \tag{24}$$

where the kth Fourier component of the particle charge density $\hat{\rho}^{p\zeta}_k$ is given by (10) through the discrete Fourier transform

$$\hat{\rho}^{p\zeta}_k = \frac{1}{N_x}\sum_{j=0}^{N_x-1}\rho^{p\zeta}_j \eta_{-k}(x_j). \tag{25}$$

Note that Eq. (24) is valid for $k \neq 0$, while for $k=0$, $\hat{E}_0 = 0$ is used to impose the total charge neutrality of the system.

Finally, Eq. (17) is used to obtain the electric field on the Eulerian grid for PIC

$$E_j = \sum_{k=-N_k}^{N_k}\hat{E}_k\eta_k(x_j). \tag{26}$$

D. Time integration

Equations (8) and (18) form a system of ordinary differential equations that can be integrated in time from a given initial condition. We apply the second-order operator splitting where linear and nonlinear terms of the Vlasov equation (1) are separated. Specifically, the linear part is

$$\frac{\partial f^\zeta}{\partial t} = \mathfrak{L}\left[f^\zeta\right] = -v\frac{\partial f^\zeta}{\partial x}, \tag{27}$$

and is treated as

$$\frac{dx^{p\zeta}_i}{dt} = v^{p\zeta}_i, \quad \frac{dv^{p\zeta}_i}{dt} = 0 \tag{28}$$

for the PIC part and as

$$\frac{dC^{s\zeta}_{n,k}}{dt} = \mathfrak{L}_{n,k}[C^{s\zeta}] \tag{29}$$

for the spectral part.

Furthermore, the nonlinear part corresponds to

$$\frac{\partial f^\zeta}{\partial t} = \mathfrak{N}\left[f^\zeta\right] = -\frac{q^\zeta}{m^\zeta}E\frac{\partial f^\zeta}{\partial v}, \quad \text{with} \quad \frac{\partial E}{\partial x} = \sum_\zeta q^\zeta\int_{-\infty}^{+\infty} f^\zeta dv. \tag{30}$$

It is treated as

$$\frac{dx^{p\zeta}_i}{dt} = 0, \quad \frac{dv^{p\zeta}_i}{dt} = \frac{q^{p\zeta}}{m^{p\zeta}}E(x^{p\zeta}_i) \tag{31}$$

for the PIC part and as

$$\frac{dC^{s\zeta}_{n,k}}{dt} = \mathfrak{N}_{n,k}[C^{s\zeta}] \tag{32}$$

for the spectral part.

Therefore, to advance the distribution function in a time step Δt, we perform the following steps:

(i) First, given the initial conditions at time $t^\theta = \theta\Delta t$, the linear part $\mathfrak{L}$ is advanced by a half time-step $\Delta t/2$ with the fully implicit Crank–Nicolson scheme.[27] For the PIC part, this yields

$$x^*_i = x^\theta_i + \frac{\Delta t}{2}\frac{v^\theta_i + v^*_i}{2}, \quad v^*_i = v^\theta_i, \tag{33}$$

where species superscripts were omitted in favor of time step, i.e., $x^\theta = x(t^\theta)$. Note that Eq. (33) reduces to the exact integration by the forward Euler method. The same time discretization for the spectral part takes the form

$$C^*_{n,k} = C^\theta_{n,k} + \frac{\Delta t}{2}\mathfrak{L}_{n,k}\left[\frac{C^* + C^\theta}{2}\right]. \tag{34}$$

The Poisson equation (24) is solved to update the electric field prior to the nonlinear step.

(ii) Next, starting from the final conditions of the previous step (labeled with superscript $*$), the time integration of the nonlinear part

$$\frac{dx^{p\zeta}_i}{dt} = 0, \quad \frac{dv^{p\zeta}_i}{dt} = \frac{q^{p\zeta}}{m^{p\zeta}}E(x^{p\zeta}_i), \tag{35}$$

$$\frac{dC^{s\zeta}_{n,k}}{dt} = \mathfrak{N}_{n,k}[C^{s\zeta}], \tag{36}$$

by a full time step Δt is performed with the standard explicit fourth-order accurate Runge–Kutta (RK) method. While the overall splitting method is second-order in temporal accuracy, it has been shown that for the nonlinear part, the fourth-order Runge–Kutta method performs better than the lower-order RK schemes (i.e., it is well balanced between –required computational steps and –permitting larger time steps).[9]

(iii) Finally, we repeat the first step (i) starting from conditions obtained at the end of (ii).

This scheme is presented in Fig. 1.

The focus of this paper is a novel discretization of a phase space. Thus far, we did not look for optimal temporal discretization leaving it for future work. Hence, to reduce the effect of the time integration, we choose sufficiently small time step in all performed tests (subsequent reduction of the time step does not change the results presented in this paper).

III. CONSERVATION PROPERTIES

The purpose of this section is to investigate the conserving properties of the hybrid method in semi-discrete setting (temporal variable is considered continuous). Similar analysis for PIC and spectral methods was heavily investigated in the past.[5,13] In general, combining the two methods may result in conservation errors that include both the errors from the original methods and coupling errors. This section shows that there is no coupling error in mass, momentum, and energy conservation associated with combining phase space discretizations.

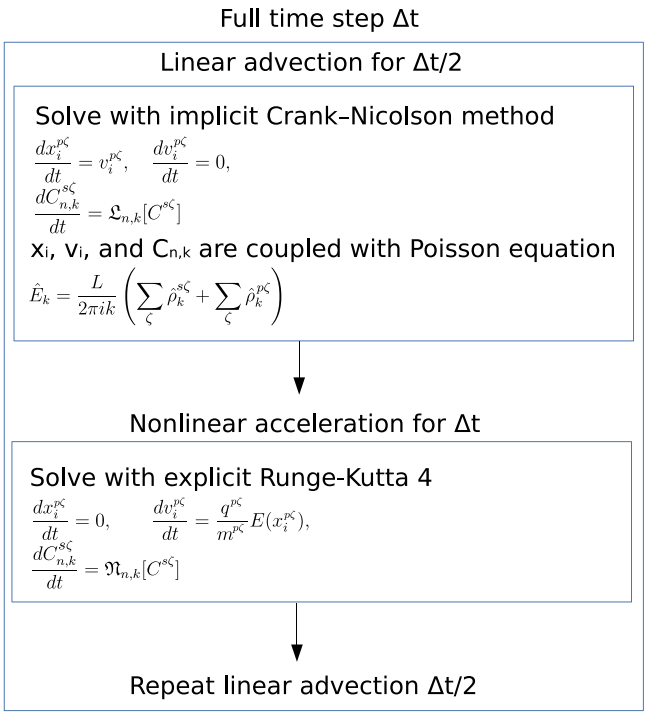

FIG. 1. Schematic representation of the time integration step.

A. Mass conservation

We will start with the trivial example of mass conservation. Obviously, the PIC conserves the total mass; thus, the error in mass conservation may only come from the spectral part. To estimate the error, we write the mass corresponding to the spectral part as follows:

$$M^s = \sum_\zeta \int_0^L \int_{-\infty}^{\infty} f^{s\zeta} dx dv = L \sum_\zeta \alpha^{s\zeta} C_{0,0}^{s\zeta}. \tag{37}$$

Since we have

$$\frac{dC_{0,0}^{s\zeta}}{dt} = 0 \quad \Rightarrow \quad \frac{dM^s}{dt} = 0, \tag{38}$$

which follows directly from the system of equations (18).

B. Momentum conservation

The second important integral of motion is total momentum. The momentum is a linear function of evolving variables; therefore, one can expect the coupling momentum error to be zero. To confirm this conjecture, we first find the particle's momentum,

$$P^p = \sum_\zeta \sum_{i=1}^{N_p^{p\zeta}} m^{p\zeta} w^{p\zeta} v_i^{p\zeta}, \tag{39}$$

and the time evolution

$$\frac{dP^p}{dt} = \sum_\zeta \Delta x \sum_{j=0}^{N_x-1} E_j \rho_j^{p\zeta} = L \sum_{k=-N_k}^{N_k} \hat{E}_{-k} \hat{\rho}_k^p, \tag{40}$$

where Eqs. (8) and (10) have been used to interpolate the particle's information on the grid. Next, the momentum of the spectral part

$$P^s = \sum_\zeta m^{s\zeta} \int_0^L \int_{-\infty}^{\infty} v f^{s\zeta} dx dv = L \sum_\zeta m^{s\zeta} \alpha^{s\zeta} \left(u^{s\zeta} C_{0,0}^{s\zeta} + \frac{\alpha^{s\zeta}}{\sqrt{2}} C_{1,0}^{s\zeta} \right).$$

Again, taking the time derivative, we note

$$\frac{dC_{1,0}^{s\zeta}}{dt} = \frac{\sqrt{2} q^{s\zeta}}{m^{s\zeta} \alpha^{s\zeta}} \sum_{k=-N_k}^{N_k} \hat{E}_{-k} C_{0,k}^{s\zeta}$$

from Eq. (18) and thus (recall, $\rho_k^{s\zeta} = C_{0,k}^{s\zeta}$)

$$\frac{dP^s}{dt} = L \sum_{k=-N_k}^{N_k} \hat{E}_{-k} \hat{\rho}_k^s. \tag{41}$$

Finally, we notice that

$$L \sum_{k=-N_k}^{N_k} \hat{E}_{-k} \hat{\rho}_k^p + L \sum_{k=-N_k}^{N_k} \hat{E}_{-k} \hat{\rho}_k^s = 2\pi i \sum_{k=-N_k}^{N_k} k |\hat{E}_k|^2 = 0, \tag{42}$$

where we have used Eq. (24) and the fact that E_{-k} and E_k are complex conjugates, which finally gives

$$\frac{d}{dt}(P^p + P^s) = 0. \tag{43}$$

Therefore, the total momentum is conserved in the semi-discrete approximation.

C. Energy conservation

The last and most complicated integral is energy. As before, we start with the particles. The kinetic energy reads

$$T^p = \frac{1}{2}\sum_\zeta \sum_{i=1}^{N_p^{p^\zeta}} m^{p^\zeta} w^{p^\zeta} (v_i^{p^\zeta})^2, \tag{44}$$

and its time derivative

$$\frac{dT^p}{dt} = \Delta x \sum_{j=0}^{N_x-1} E_j J_j^{p^\zeta} = L \sum_{k=-N_k}^{N_k} \hat{E}_{-k} \hat{J}_k^p, \tag{45}$$

which is obtained similarly to Eq. (40), with current and its Fourier transform defined as

$$J_j^p = \frac{1}{\Delta x}\sum_\zeta \sum_{i=1}^{N_p^{p^\zeta}} q^{p^\zeta} v_i^{p^\zeta} w^{p^\zeta} S(x_i - x_j), \tag{46}$$

$$\hat{J}_k^p = \frac{1}{N_x}\sum_\zeta \sum_{j=0}^{N_x-1} J_j^{p^\zeta} \exp\left(-2\pi i \frac{k x_j}{L}\right). \tag{47}$$

Next, the kinetic energy of the spectral part

$$\begin{aligned} T^s &= \frac{1}{2}\sum_\zeta m^{s^\zeta} \int_0^L \int_{-\infty}^{\infty} v^2 f^{s^\zeta} dx dv \\ &= \frac{L}{2}\sum_\zeta \alpha^{s^\zeta} m^{s^\zeta} \left(\left((u^{s^\zeta})^2 + \frac{(\alpha^{s^\zeta})^2}{2} \right) C_{0,0}^{s^\zeta} \right. \\ &\quad \left. + \sqrt{2}\alpha^{s^\zeta} u^{s^\zeta} C_{1,0}^{s^\zeta} + \frac{(\alpha^{s^\zeta})^2}{\sqrt{2}} C_{2,0}^{s^\zeta} \right). \end{aligned} \tag{48}$$

Again, the time derivative components are obtained with Eq. (18) and yields

$$\frac{dT^s}{dt} = L \sum_{k=-N_k}^{N_k} \hat{E}_{-k} \hat{J}_k^s, \tag{49}$$

with the total current defined as

$$\hat{J}_k^s = \sum_\zeta q^{s^\zeta} \alpha^{s^\zeta} \left(u^{s^\zeta} C_{0,k}^{s^\zeta} + \frac{\alpha^{s^\zeta}}{\sqrt{2}} C_{1,k}^{s^\zeta} \right). \tag{50}$$

Now, the electrostatic energy

$$\Pi = \int \frac{E^2}{2} dx = \frac{L}{2} \sum_{k=-N_k}^{N_k} |\hat{E}_k|^2, \tag{51}$$

and the time derivative

$$\frac{d}{dt}\Pi = -L \sum_{k=-N_k}^{N_k} \hat{E}_{-k} \hat{\mathfrak{J}}_k^p - L \sum_{k=-N_k}^{N_k} \hat{E}_{-k} \hat{\mathfrak{J}}_k^s, \tag{52}$$

where we defined

$$\hat{\mathfrak{J}}_k^{s'} = -\frac{L}{2\pi i k} \frac{d\hat{\rho}_k^{s'}}{dt}, \text{ for } s' \in \{s, p\}. \tag{53}$$

Note that the change in potential energy as shown in Eq. (52) does not have any cross-terms and thus there are no coupling effects when combining the spectral and particle methods in the given approach for energy conservation. Assembling all the terms together, we have

$$\frac{d}{dt}(T^s + T^p + \Pi) = \epsilon^s + \epsilon^p. \tag{54}$$

The error contribution from the spectral method is zero

$$\epsilon^s = L \sum_{k=-N_k}^{N_k} \hat{E}_{-k} \left(\hat{J}_k^s - \hat{\mathfrak{J}}_k^s \right) = 0, \tag{55}$$

because

$$\hat{\mathfrak{J}}_k^s = -\sum_\zeta \frac{L}{2\pi i k} \frac{d\rho_k^{s^\zeta}}{dt} = -\sum_\zeta q^{s^\zeta} \alpha^{s^\zeta} \frac{L}{2\pi i k} \frac{dC_{0,k}^{s^\zeta}}{dt} = \hat{J}_k^s, \tag{56}$$

where the time derivative of $C_{0,k}$ is obtained from the system of equations (18) and J_k^s is defined in Eq. (50). Finally, the error contribution from particles is generally not zero

$$\epsilon^p = L \sum_{k=-N_k}^{N_k} \hat{E}_{-k} \left(\hat{J}_k^p - \hat{\mathfrak{J}}_k^p \right). \tag{57}$$

One can change the particle shape function, so that $\hat{J}_k^p = \hat{\mathfrak{J}}_k^p$ to conserve energy. However, this will result in a method that does not conserve momentum similarly to classical PIC codes; cf. Ref. 5. At the same time, a gridless formulation of PIC that relies on Fourier basis in space can offer both momentum and energy conservation.[28] With unequally spaced fast Fourier transform algorithms,[29,30] it can achieve efficiency close to that of the classical PIC with FFT. Alternatively, a hybrid grid treatment was proposed in Ref. 31, with a Lagrangian treatment of the particle's velocity and a Eulerian approach for all of the spatial dynamics; it achieves the conservation of momentum and energy simultaneously. However, since we focus on the efficient velocity space discretization, in this work, we have utilized the classical PIC approach based on its widespread use and the ease of implementation. A fully conservative hybrid method is left for future work.

It is important to note that the conservation of energy in the spectral method that follows from Eq. (55) will hold with an implicit time discretization scheme such as the implicit midpoint method[16] and will not hold for the operator splitting scheme utilized in this work.

IV. RESULTS

In this section, we compare the hybrid method against the fully spectral method for the example of a weak electron beam propagating in a plasma, with the beam density $n_{beam} = 10^{-2}$. In the case of low beam density, this problem requires highly accurate methods and is challenging for conventional PIC methods because the timescale required to reach the saturated state is long, proportional to $1/n_{beam}$,[32] and because the instability saturates at relatively small amplitudes. Thus, it becomes computationally expensive to achieve satisfactory accuracy and may require specific initialization techniques to keep the statistical noise level low. On the other hand, in the spectral method, a high number of Hermite polynomials might be required to capture the correct system dynamics because the distribution function forms a

plateau in the velocity space, which significantly deviates from a Maxwellian distribution.

Given these considerations, our goal is to use this problem as a test-bed to determine whether the hybrid method could be a good compromise between a high accuracy noiseless spectral approach and a particle method, which works well for arbitrarily complicated distribution functions.

Two similar test cases are considered that differ only in the system length and resolution. First, a "single-mode" test where system size L is approximately equal to the most unstable mode wavelength λ_{inst}, i.e., $L \approx \lambda_{inst} = 2\pi/k_{\text{inst}}$ with $k_{\text{inst}} \approx \omega_{pe}/v_{\text{mean}}$ (recall, $\omega_{pe} = 1$ due to the normalization), where v_{mean} is the mean velocity of electron beam. In this case, the deviation of the initial velocity distribution function from Maxwellian is not too severe. For the second test case, we increase the domain size ($L = 30\lambda_{inst}$) to resolve the spectrum of linearly unstable modes (excite ten of them simultaneously) and expect the distribution function to flatten due to quasi-linear interactions. In this case, we show that the hybrid method with particle treatment of the electron beam captures the linear regime with a good accuracy and develops a plateau in the velocity space during the nonlinear stage. Due to severe deviation of the beam distribution from Maxwellian, the fully spectral method based on AWH basis (well suited to near-Maxwellian behavior) fails in the early nonlinear stage, with its coefficients diverging for the resolution considered. Dynamic change of free parameters α, u for AWH basis functions is known to improve convergence,[33] or control global stability in terms of L_2-norm by a time-dependent scaling function,[34] but these topics are beyond the scope of this paper; thus, we omit comparison of the hybrid and the spectral methods in the case of multiple linearly unstable modes.

A. Problem setup and initialization

Here, we outline the parameters common to both test cases. We consider a spatially uniform plasma consisting of three particle species, bulk ions (singly-charged protons with zero mean velocity), bulk electrons (electrons with zero mean velocity), and beam electrons (small portion of electrons with high mean velocity). The detailed parameters for each particle species are listed in Table I, following the normalization described in Sec. II. We initialize all species with Maxwellian distribution functions of different mean velocities ($v_{mean} = 0$ for the bulk and $v_{\text{mean}} = v_{\text{beam}} = 10$ for the beam). The electron temperature is the same for bulk and beam electrons, $T_e = 1$, while ions are colder, $T_i = 0.1$.

The initial electron distribution function is

$$f^e(t=0,x,v) = \frac{(1-n_{beam})}{\sqrt{2\pi}}\exp\left(-\frac{v^2}{2}\right) + \frac{n_{beam}}{\sqrt{2\pi}}\exp\left(\frac{-(v-10)^2}{2}\right), \tag{58}$$

TABLE I. Physical parameters for different species.

Parameters\Species	Bulk ions	Bulk electrons	Beam electrons
Charge	1	−1	−1
Mass	1836	1	1
Mean velocity	0	0	10
Temperature	0.1	1	1
Density	1	$1 - n_{beam}$	n_{beam}

where the bulk electrons are initialized by setting $C^{s,bulk}_{0,0} = (1 - n_{beam})/\alpha^{bulk}$ with $\alpha^{bulk} = \sqrt{2}, u^{bulk} = 0$. Note that only one spectral coefficient is sufficient to represent the initial Maxwellian distribution function in the velocity space (the initial perturbation in space for each numerical case is described below). The electron beam is initialized similarly, by setting $C^{s,beam}_{0,0} = n_{beam}/\alpha^{beam}$ in the spectral method with $\alpha^{beam} = \sqrt{2}, u^{beam} = 10$, and in the hybrid method by sampling particle velocities from a pseudorandom number sequence. The ion distribution function is initialized with $C^{s,i}_{0,0} = 1/\alpha^i$, where $\alpha^i = \sqrt{0.2/1836}, u^i = 0$.

B. Single-mode configuration

In order to compare hybrid and spectral methods, two types of simulations are performed. In all simulations, the bulk ions and electrons are treated with the spectral method, where the number of Hermite polynomials is fixed at $N_v = 64$. A reference solution is obtained by using the fully spectral method where the electron beam is resolved with $N_v = 4096$ Hermite modes. At the same time, the hybrid method represents the electron beam with the PIC technique, where the number of beam particles per computational cell is varied as $N_p = 32, 128, 512, 2048, 8192$. The collisional frequency ν for the bulk ions and electrons in all single-mode simulations is set to 1 and 50, while for the electron beam in the reference solution to 150 (the values are chosen to keep the solutions stable while not interfering with physical results and convergence properties). Note that the collision factor $\nu g(n)$ given in Eq. (18) is approximately $\nu n^3/N_v^3$, and with the collision frequency $\nu = 150$ for electron beam in the reference solution, its value is 0.29 for the mode number $N_v = 512$, and it decreases at a cubic rate for lower mode numbers.

The parameters common to the spectral and hybrid methods are the following: the time step is $\Delta t = 0.0125$, with the total simulation time $T = 150$; the domain length is $L = 20\pi$; the number of spatial grid points is $N_x = 65$. The time step was chosen to resolve the plasma frequency, $\omega_{pe}\Delta t \ll 1$ and to be small enough not to significantly contribute to numerical error (vs phase space discretization error). The spatial resolution was chosen to cover the most unstable wavenumbers (i.e., near the Landau resonance) and to resolve the Debye length, $k\lambda_D \approx 1$. Convergence studies were performed to ensure that time and space discretization errors do not significantly affect the results of this section and are small in comparison with velocity space discretization errors (not shown).

In this case, a single unstable mode $kL/2\pi = 1$ is perturbed for the bulk electron density as

$$C^{s,bulk}_{n=0,1} = \epsilon\Omega_1, \quad C^{s,bulk}_{n=0,-1} = \left(C^{s,bulk}_{n=0,1}\right)^*, \tag{59}$$

with the amplitude $\epsilon = 10^{-4}$, and the phase is defined by the complex number $\Omega_1 = 0.5 + i0.5$ used in both hybrid and spectral simulations. Here, the superscript * refers to complex conjugate.

1. Diagnostics

In order to quantify the merits of the two simulation approaches, we define errors in the distribution function and the electric field to be

$$\varepsilon_f = \sqrt{\frac{\int_{v_{min}}^{v_{max}} |f(v) - f^{\text{ref}}(v)|^2 dv}{\int_{v_{min}}^{v_{max}} |f^{\text{ref}}(v)|^2 dv}}, \tag{60}$$

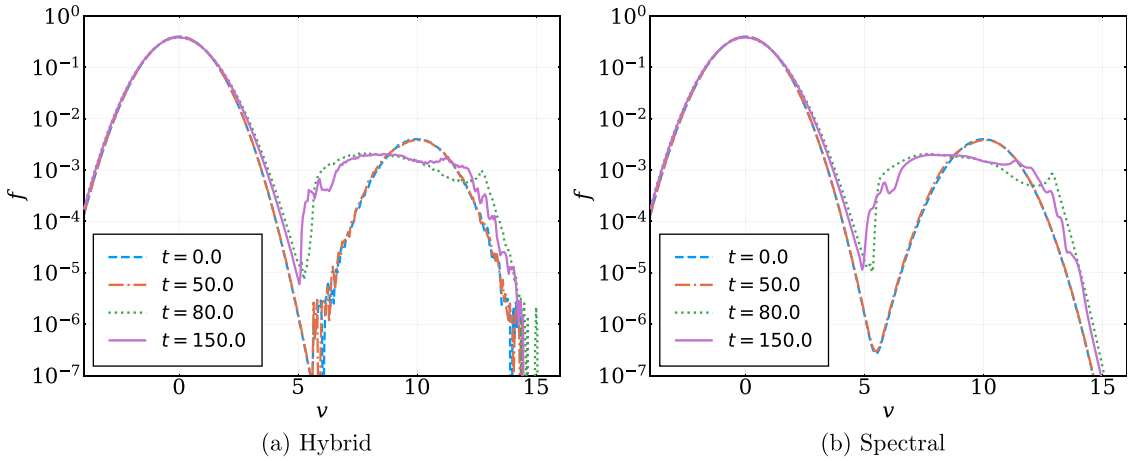

FIG. 2. (a) Evolution of the electron distribution function using the hybrid method with $N_p = 2048$ resolving beam and (b) the fully spectral method, the reference solution with $N_v = 4096$ for the beam.

$$\varepsilon_E = \sqrt{\frac{\sum_{k=0}^{N_k} ||\hat{E}_k| - |\hat{E}_k^{\text{ref}}||^2}{\sum_{k=0}^{N_k} |\hat{E}_k^{\text{ref}}|^2}}, \tag{61}$$

where $[v_{min}, v_{max}]$ is the velocity range for which the distribution function error is computed, $f^{\text{ref}}(v)$, $\hat{E}_k^{\text{ref}}$ are the velocity distribution function and the electric field for the reference solution, averaged over the time interval $T = [125, 150]$ (nonlinear stage). The spatial dependence of the distribution function is removed by the integration [i.e., $f(v) = 1/L \int_0^L f(x, v)dx$].

2. Single-mode results

The configuration described above is unstable to the beam–plasma instability driven by the positive slope (i.e., inverse Landau damping) of the electron beam distribution function. The evolution of the electron distribution function obtained by the hybrid method ($N_p = 2048$) is shown in Fig. 2(a), where the plateau is formed shortly in the nonlinear regime, at $t \approx 80$. The spectral method result for the reference solution ($N_v = 4096$) is shown in Fig. 2(b).

The linear phase is in good agreement with the theoretically predicted growth rate computed to be $\gamma = 0.089\,78$ for $kL/2\pi = 1$ from the classical dispersion relation of the kinetic beam–plasma instability,[35]

$$1 - \frac{1}{2k^2} \sum_j \frac{n_j}{T_j} Z'\left(\frac{\omega - k v_{\text{mean},j}}{k\sqrt{2}} \sqrt{\frac{m_j}{T_j}}\right) = 0, \tag{62}$$

where the sum is over different plasma species (bulk electrons, beam electrons, and ions), $v_{\text{mean},j}$ is the mean velocity of j-specie, $\omega = \omega_{Re} + i\gamma$ is the complex frequency, and

$$Z'(x) = \sqrt{\pi} \int_{-\infty}^{\infty} dt \frac{e^{-t^2}}{(t - x)^2}$$

is the derivative of the plasma dispersion function. Figure 3 shows the hybrid and the fully spectral solutions for the time evolution of the electrostatic mode $|E_1|$, where good agreement between the two is observed. For a low number of particles in the hybrid method, $N_p \approx 32$, the amplitude of the statistical noise interferes with the linear stage of the instability and results in a faster growth and nonlinear saturation.

It is shown in Sec. III that the hybrid method in a semi-discrete setting conserves mass and momentum, but not the total energy of the system. The mass conservation is observed to be exact (not shown), the coefficient $C^s_{0,0} = \text{const}$ for the spectral representation, and the number of particles remains constant in the periodic setup. Figures 4(a) and 4(b) demonstrate the relative change in the total momentum and energy for the hybrid and the fully spectral (reference) simulations. As expected from Sec. III, the total momentum is conserved for both spectral and hybrid methods. The energy error for the reference solution comes only due to the time-stepping algorithm, which

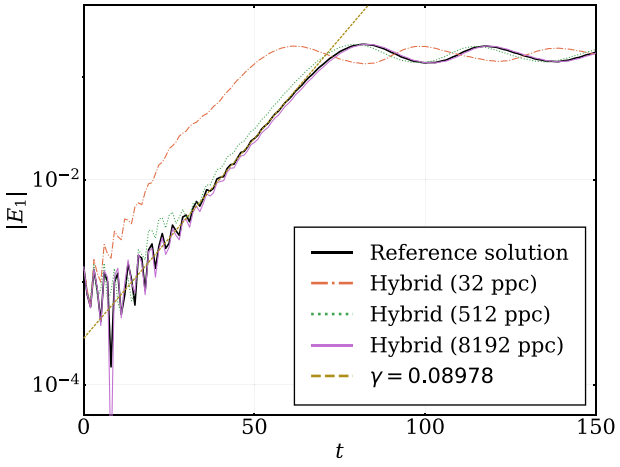

FIG. 3. Evolution and the growth rate of the unstable mode $kL/2\pi = 1$ for the electrostatic field for the case with single-mode dynamics.

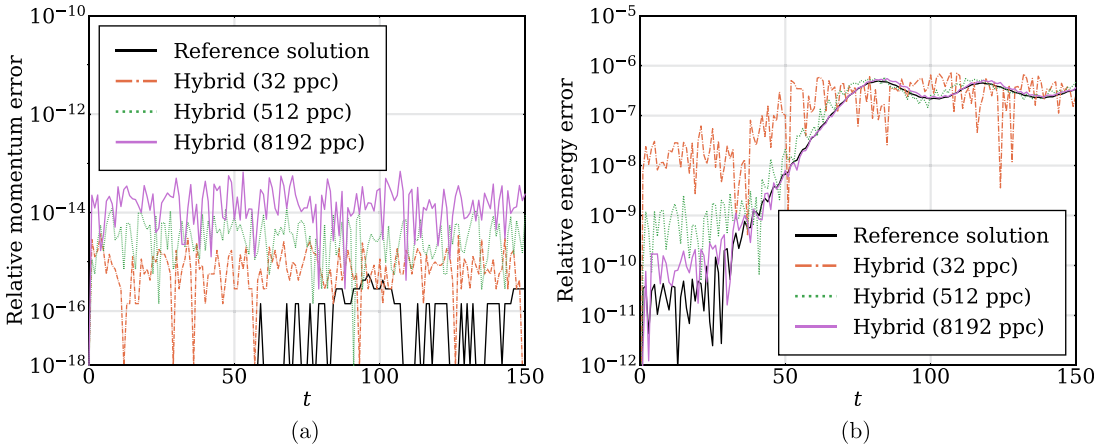

FIG. 4. (a) Relative change of momentum and (b) energy from its initial values for the hybrid solutions and the fully spectral (reference) solution.

is not energy conserving, while for the hybrid method, the PIC method also contributes to the error, which scales with the number of particles.

Finally, we demonstrate the convergence of the hybrid method by comparing it to the reference solution. The relative error in the electron distribution function with an increased number of particles resolving electron beam is shown in Fig. 5. Not surprisingly, the biggest error comes from the PIC representation. The error in the electrostatic field is shown in Fig. 6(a), and the error in the distribution function in Fig. 6(b), defined in Eqs. (61) and (60), respectively. The error in the distribution function is calculated in the velocity domain with boundaries $[v_{min}, v_{max}] = [-4, 14]$. Both errors scale with the number of particles as $\sim 1/\sqrt{N_p}$, which is expected for particle-in-cell methods with standard velocity loading algorithms. The variability of reported errors is likely due to a lack of ensemble-averaged results, which can be obtained with repeated hybrid simulations with various randomizations of the initial particle loading.

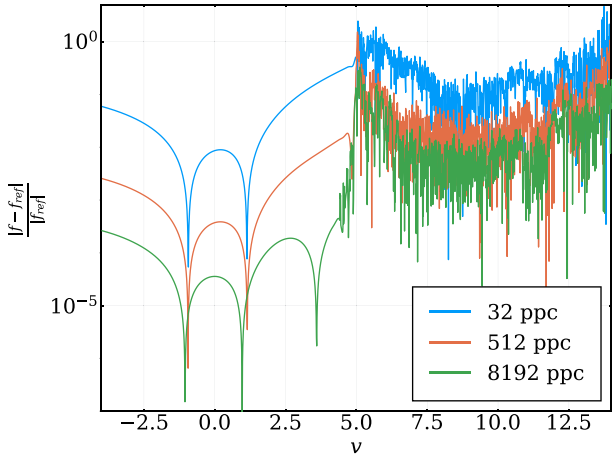

FIG. 5. Relative error of the electron distribution function between the hybrid method with variable number of particles in the electron beam and the reference solution.

C. Multiple-mode configuration

Here, we provide the parameters for the hybrid method only: the number of spectral modes is $N_v = 16$ for bulk ions and electrons, while the collision frequency is set to $\nu = 10$ for bulk electrons and $\nu = 1$ for the bulk ions. The system length is $L = 2048$ to resolve multiple linearly unstable modes, and the number of spatial grid points is set to $N_x = 2049$.

1. Initial perturbation

In order to drive the dynamics of the system, we perturb the bulk electron density as

$$C^{s,bulk}_{n=0,k} = \frac{\epsilon \Omega_k k}{k_{min}}, \quad C^{s,bulk}_{n=0,-k} = \left(C^{s,bulk}_{n=0,k}\right)^*, \tag{63}$$

for $k \in [k_{min}, k_{max}]$, corresponding approximately to the most unstable modes. Here, $\epsilon = 10^{-4}$ is the perturbation amplitude, $k_{min} = 32$, $k_{max} = 42$ is the range of perturbed modes, $|\Omega_k| = 1$ is a complex number with the unit amplitude and the random phase. Therefore, all perturbed modes are initialized with the same amplitude of electric field while their phases are randomized. Note, in both hybrid and spectral simulations, the phase for each mode is the same to ensure equivalent initial conditions.

2. Multi-mode results

The case with multiple linearly unstable modes is highly turbulent, and the instability generates Langmuir waves at the expense of beam energy. Eventually, waves start to disrupt the beam, removing the instability source and flattening the positive slope of the distribution function. At later times, the electron distribution function develops a plateau and the instability saturates. It is worth mentioning that one could obtain a reference solution via a statistical approach in this case (loading particles using different pseudorandom number sequences). The evolution of the electron distribution function obtained by the hybrid method with $N_p = 2048$ is shown in Fig. 7(a). In terms of the electric field power spectrum, after a short initial transient, the unstable modes ($kL/2\pi \approx 32 - 42$) grow. Due to nonlinear

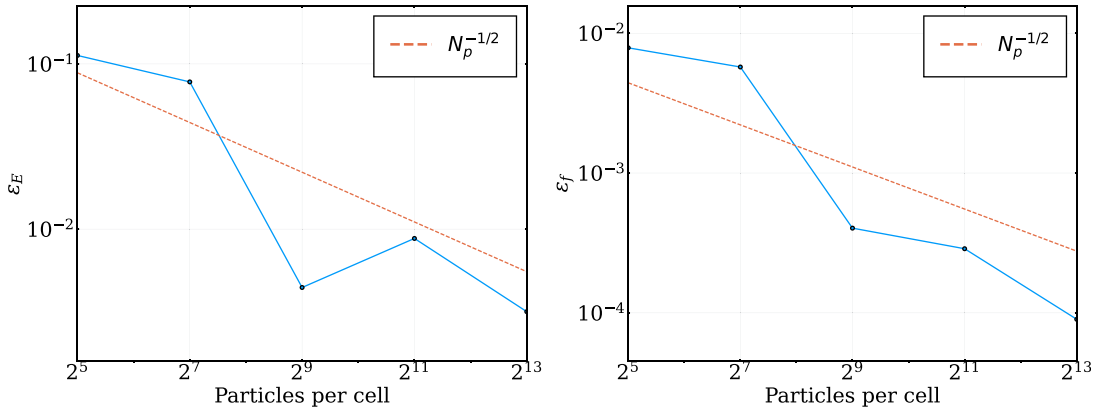

(a) (b)

FIG. 6. (a) Error in the electrostatic field and (b) the distribution function between hybrid simulations and the reference solution with various numbers of particles resolving electron beam, calculated on the velocity domain $[v_{min}, v_{max}] = [-4, 14]$.

wave–wave interactions, energy cascades into other regions of the spectrum forming the profile shown in Fig. 7(b).

At the same time, the evolution of a single mode with $kL/2\pi = 36$ is shown in Fig. 8(a), where one can see the linear growth phase smoothly transitioning into nonlinear saturation. Note that the linear regime is reproduced accurately even with a relatively low number of particles in the hybrid method, and using a standard particle loading technique. The wave-particle resonance nature of the instability is sensitive to noise present in the initial distribution function near the resonance velocities, and typically particle methods require special techniques such as "quiet" loading (utilizing the so-called low-discrepancy sequence instead of pseudorandom sequences),[5,36] δf method,[37–39] etc. The hybrid method presented here offers an alternative approach, describing highly non-equilibrium dynamics with the particle method and the near-Maxwellian population with the spectral method.

The growth rates of excited modes were measured during the linear stage and are presented in Fig. 8(b) in comparison with theoretical predictions by Eq. (62). In the absence of a reference solution, the convergence of the growth rate values with the number of particles serves as a verification of these simulations.

It is expected that harmonic Langmuir waves are excited during the beam–plasma interaction.[40] The electric field power spectra in Fig. 9 show clearly the presence of the Langmuir waves and their harmonics, obtained via the hybrid method with $N_p = 128$ and a longer simulation time.

Finally, Figs. 10(a) and 10(b) demonstrate the relative change in the total momentum and energy. Similar to the previous case, the total momentum is well conserved, while the total energy is not conserved. However, the relative energy error is quite small, even when 32 particle-per-cell are considered.

V. DISCUSSION AND CONCLUSION

We have presented a numerical hybrid method that combines spectral and particle approaches for velocity space discretizations of the solution of the Vlasov–Maxwell equations. We have demonstrated its application on the one-dimensional electrostatic problem by solving

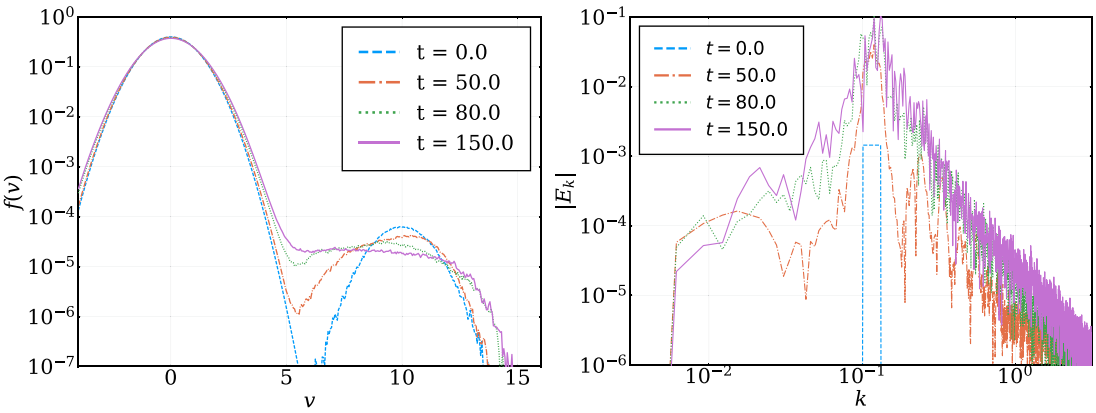

(a) Distribution function (b) Electric field

FIG. 7. (a) Evolution of the electron distribution function and (b) the electric field spectrum for the case with the multiple mode dynamics obtained with the hybrid method with $N_p = 2048$.

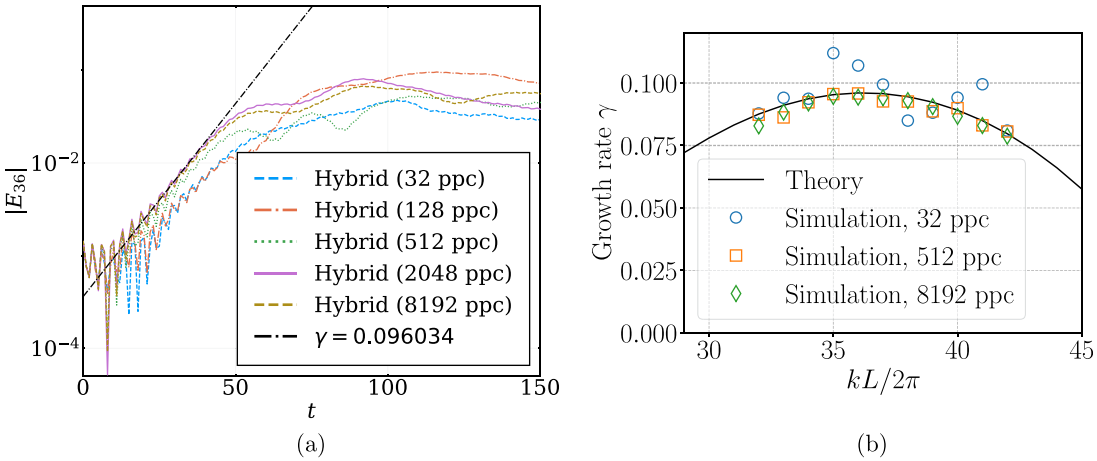

FIG. 8. (a) Evolution and the growth rate of the unstable mode $kL/2\pi = 36$ for the electrostatic field, (b) comparison between the theoretical growth rate solving Eq. (62) and growth rates measured in the simulations.

the Vlasov–Poisson equations. A particle-in-cell method was used for the particle approach and asymmetrically weighted Hermite basis functions for the spectral method, with space discretized using Fourier basis functions. We have analyzed conservation properties of the given hybrid approach and showed the absence of a coupling error between the two combined methods in the semi-discrete setting (where the temporal variable remains in the continuum).

We have designed configurations for numerical tests simulating interaction between a weak electron beam and a background plasma with the beam evolving into a highly non-equilibrium state. This problem is hard for both PIC and spectral methods, as it would require much particles per cell or much spectral terms to capture the turbulent

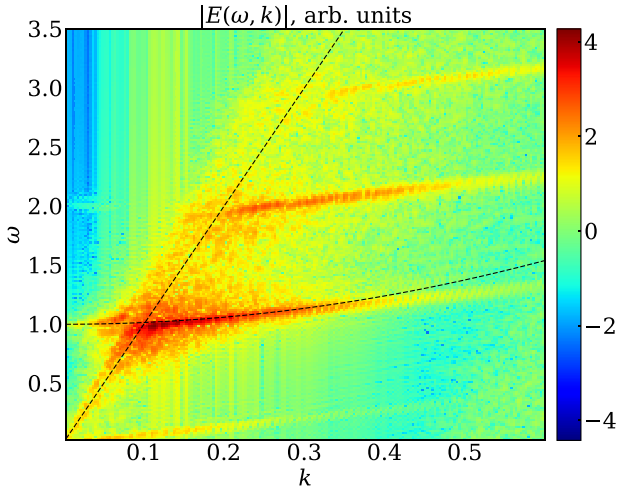

FIG. 9. Electric field power spectra for the case with multiple-mode dynamics obtained using the hybrid method with $N_p = 128$. Black dashed lines represent the dispersion relation for the electron plasma waves $\omega = 1 + 1.5k^2$ and the electron beam $\omega = kv_0$. A two-dimensional Hamming window function (designed as the outer product of two one-dimensional functions) has been superimposed on the electric field signal.

saturated state and the plateau in the distribution function accurately. The hybrid method inherits the scalings of errors of the PIC technique, since PIC is a lower-order method relative to the spectral approach, but the overall accuracy of the simulation is higher than what it would be if one adopted a standard PIC approach alone (noise is effectively reduced by $n_{Beam}/n_{Bulk} \ll 1$ factor). On the other hand, it also gives much flexibility for very non-Maxwellian distribution functions, such as the quasi-linear plateau originating from the beam–plasma instability considered in this paper, which would be hard to model accurately with a Hermite-based spectral approach, which is intimately related to Maxwellian distribution functions and hence is more suited to capture near-Maxwellian behavior. Indeed, the tests presented in Sec. IV illustrate the potential of the hybrid method, which achieves good accuracy in both linear and nonlinear stages of the beam–plasma instability despite a relatively low growth rate (electron beam density is orders of magnitude lower than the bulk plasma density), even when using a relatively low number of particles per cell.

Some parallels of the presented method could be drawn with the so-called δf method,[37,38] except that in the present formulation, both the beam (δf) and the bulk (f_0) are evolved self-consistently and coupled only through electromagnetic fields. While one can construct a δf method with evolving background plasma, e.g., by solving plasma fluid equations to evolve the bulk,[41] or remapping information to/from the bulk dynamically,[42,43] our hybrid method offers an alternative approach where the beam is described with a standard PIC method. Furthermore, AWH basis functions for the bulk plasma are linked to the moments of the plasma fluid equations,[44] which offers more flexibility to the bulk representation. While we did not attempt to vary the number of spectral modes and particles dynamically, this can be beneficial, especially for more diffusive cases where an equilibrium is reached, such as in asymptotically complexity diminishing schemes.[45]

The examples presented in this work illustrate the decomposition in velocity space; however, one can easily imagine problems where the decomposition in the configuration space may also be needed, i.e., in problems of highly localized phenomena (such as shocks, reconnection, etc.). In these cases, the decomposition will be similar to fluid simulations with embedded kinetic regions.[46–48] Thus, the great

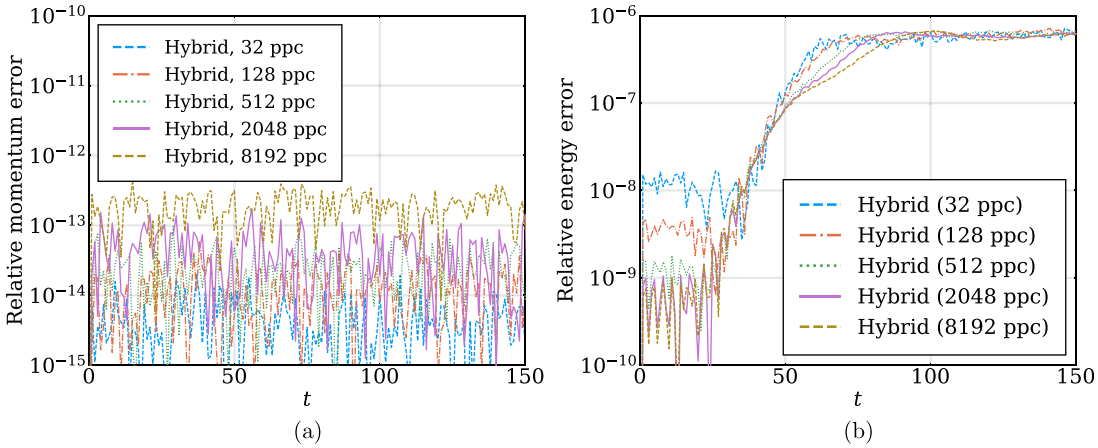

FIG. 10. Relative change of (a) momentum and (b) energy from its initial values for the hybrid solutions with multiple-mode dynamics.

flexibility to treat different parts of the phase space with different methods or even with the same method but different resolution is the virtue of the proposed method.

Finally, we would like to mention that the hybrid method presented here was implemented serially, but it is important to discuss its parallelization capabilities. The hybrid method in this work was implemented with a spectral Fourier method for spatial coordinates, which is known to have poor parallel scaling on distributed systems due to its global nature. Similarly to Ref. 13 with a fully spectral Hermite–Fourier method, we suggest that an efficient parallelization for the hybrid method can also be achieved by domain decomposition in velocity space [note the tridiagonal structure of the linear operator in Eq. (19)]. Moreover, the particle component can be efficiently integrated in parallel with the communications needed once per time step to gather the charge density. The authors suggest that a high parallel efficiency can be achieved with discretizations that have a "shorter stencil size" in the spatial domain, such as finite difference or finite elements; e.g., see Ref. 49.

ACKNOWLEDGMENTS

The authors acknowledge discussions with Gianmarco Manzini. This work was supported by the Laboratory Directed Research and Development Program of the Los Alamos National Laboratory under Project Nos. 20170207ER and 20220104DR. The Los Alamos National Laboratory is operated by Triad National Security, LLC, for the National Nuclear Security Administration of the U.S. Department of Energy (Contract No. 89233218CNA000001). Computational resources for the simulations were provided by the Los Alamos National Laboratory Institutional Computing Program.

AUTHOR DECLARATIONS

Conflict of Interest

The authors have no conflicts to disclose.

Author Contributions

Oleksandr Chapurin: Conceptualization (equal); Data curation (lead); Formal analysis (equal); Investigation (lead); Methodology (supporting); Software (supporting); Validation (lead); Visualization (lead); Writing – original draft (equal); Writing – review & editing (lead). **Oleksandr Koshkarov:** Conceptualization (lead); Formal analysis (equal); Investigation (lead); Methodology (equal); Project administration (equal); Software (lead); Supervision (equal); Validation (equal); Visualization (supporting); Writing – original draft (equal); Writing – review & editing (equal). **Gian Luca Delzanno:** Conceptualization (lead); Funding acquisition (equal); Investigation (equal); Methodology (equal); Project administration (equal); Supervision (equal); Validation (equal); Writing – review & editing (lead). **Vadim Roytershteyn:** Conceptualization (lead); Software (equal); Supervision (supporting); Writing – review & editing (equal). **Peter T. Brady:** Conceptualization (equal); Writing – review & editing (equal). **Robert Chiodi:** Conceptualization (equal); Writing – review & editing (equal). **Cale Harnish:** Conceptualization (equal); Writing – review & editing (equal). **Daniel Livescu:** Conceptualization (equal); Funding acquisition (equal); Writing – review & editing (equal).

DATA AVAILABILITY

The data that support the findings of this study are available from the corresponding author upon reasonable request.

REFERENCES

[1]M. Aschwanden, *Physics of the Solar Corona* (Springer Praxis Books, Springer Berlin Heidelberg, 2005).
[2]D. Biskamp, *Magnetic Reconnection in Plasmas, Cambridge Monographs on Plasma Physics* (Cambridge University Press, 2009).
[3]R. Bruno and V. Carbone, "The solar wind as a turbulence laboratory," Living Rev. Sol. Phys. **12**, 4 (2005).
[4]G. D. Reeves, H. E. Spence, M. G. Henderson, S. K. Morley, R. H. W. Friedel, H. O. Funsten, D. N. Baker, S. G. Kanekal, J. B. Blake, J. F. Fennell, S. G. Claudepierre, R. M. Thorne, D. L. Turner, C. A. Kletzing, W. S. Kurth, B. A. Larsen, and J. T. Niehof, "Electron acceleration in the heart of the Van Allen radiation belts," Science **341**, 991 (2013).
[5]C. K. Birdsall and A. B. Langdon, *Plasma Physics via Computer Simulation* (CRC Press, 2004).
[6]T. P. Armstrong, R. C. Harding, G. Knorr, and D. Montgomery, "Solution of Vlasov's equation by transform methods," Methods Comput. Phys. **9**, 29–86 (1970).

[7]M. Shoucri and R. R. J. Gagne, "Numerical solution of the Vlasov equation by transform methods," J. Comput. Phys. **21**(2), 238–242 (1976).
[8]J. P. Holloway, "Spectral velocity discretizations for the Vlasov-Maxwell equations," Transp. Theory Stat. Phys. **25**(1), 1–32 (1996).
[9]J. W. Schumer and J. P. Holloway, "Vlasov simulations using velocity-scaled Hermite representations," J. Comput. Phys. **144**(2), 626–661 (1998).
[10]Z. Cai, Y. Fan, and R. Li, "Globally hyperbolic regularization of Grad's moment system," Commun. Pure Appl. Math. **67**(3), 464–518 (2014).
[11]Z. Cai and Y. Wang, "Suppression of recurrence in the Hermite-spectral method for transport equations," SIAM J. Numer. Anal. **56**(5), 3144–3168 (2018).
[12]Y. Di, Y. Fan, Z. Kou, R. Li, and Y. Wang, "Filtered hyperbolic moment method for the Vlasov equation," arXiv:1712.06433 (2018).
[13]G. Delzanno, "Multi-dimensional, fully-implicit, spectral method for the Vlasov–Maxwell equations with exact conservation laws in discrete form," J. Comput. Phys. **301**, 338–356 (2015).
[14]J. Vencels, G. L. Delzanno, G. Manzini, S. Markidis, I. B. Peng, and V. Roytershteyn, "Spectral plasma solver: A spectral code for multiscale simulations of collisionless, magnetized plasmas," J. Phys.: Conf. Ser. **719**, 012022 (2016).
[15]G. Manzini, G. Delzanno, J. Vencels, and S. Markidis, "A Legendre–Fourier spectral method with exact conservation laws for the Vlasov–Poisson system," J. Comput. Phys. **317**, 82–107 (2016).
[16]E. Camporeale, G. Delzanno, B. Bergen, and J. Moulton, "On the velocity space discretization for the Vlasov–Poisson system: Comparison between implicit Hermite spectral and Particle-in-Cell methods," Comput. Phys. Commun. **198**, 47–58 (2016).
[17]C. Z. Cheng and G. Knorr, "The integration of the Vlasov equation in configuration space," J. Comput. Phys. **22**(3), 330–351 (1976).
[18]E. Sonnendrücker, J. Roche, P. Bertrand, and A. Ghizzo, "The semi-Lagrangian method for the numerical resolution of the Vlasov equation," J. Comput. Phys. **149**(2), 201–220 (1999).
[19]F. Filbet, E. Sonnendrücker, and P. Bertrand, "Conservative numerical schemes for the Vlasov equation," J. Comput. Phys. **172**(1), 166–187 (2001).
[20]A. Christlieb, W. Guo, M. Morton, and J.-M. Qiu, "A high order time splitting method based on integral deferred correction for semi-Lagrangian Vlasov simulations," J. Comput. Phys. **267**, 7–27 (2014).
[21]Y. Cheng, A. J. Christlieb, and X. Zhong, "Energy-conserving discontinuous Galerkin methods for the Vlasov–Maxwell system," J. Comput. Phys. **279**, 145–173 (2014).
[22]J. Juno, A. Hakim, J. TenBarge, E. Shi, and W. Dorland, "Discontinuous Galerkin algorithms for fully kinetic plasmas," J. Comput. Phys. **353**, 110–147 (2018).
[23]R. Hockney and J. Eastwood, *Computer Simulation Using Particles* (Taylor & Francis, 1988).
[24]J. P. Boyd, *Chebyshev and Fourier Spectral Methods: Second Revised Edition*, Dover Books on Mathematics (Dover Publications, 2001).
[25]S. A. Orszag, "Numerical simulation of incompressible flows within simple boundaries. 1. Galerkin (spectral) representations," Stud. Appl. Math. **50**(4), 293–327 (1971).
[26]J. W. Cooley and J. W. Tukey, "An algorithm for machine calculation of complex Fourier series," Math. Comput. **19**(90), 297–301 (1965).
[27]J. Crank and P. Nicolson, "A practical method for numerical evaluation of solutions of partial differential equations of the heat-conduction type," Adv. Comput. Math. **6**(1), 207–226 (1996).
[28]M. S. Mitchell, M. T. Miecnikowski, G. Beylkin, and S. E. Parker, "Efficient Fourier basis particle simulation," J. Comput. Phys. **396**, 837–847 (2019).
[29]G. Beylkin, "On the fast Fourier transform of functions with singularities," Appl. Comput. Harmonic Anal. **2**(4), 363–381 (1995).
[30]A. Dutt and V. Rokhlin, "Fast Fourier transforms for nonequispaced data," SIAM J. Sci. Comput. **14**(6), 1368–1393 (1993).
[31]T. Shiroto, A. Matsuyama, and M. Yagi, "A charge-momentum-energy-conserving 1D3V hybrid Lagrangian–Eulerian method for Vlasov–Maxwell system," J. Comput. Phys. **469**, 111522 (2022).
[32]H. Ratcliffe, C. S. Brady, M. B. Che Rozenan, and V. M. Nakariakov, "A comparison of weak-turbulence and particle-in-cell simulations of weak electron-beam plasma interaction," Phys. Plasmas **21**(12), 122104 (2014).
[33]C. Pagliantini, G. L. Delzanno, and S. Markidis, "Physics-based adaptivity of a spectral method for the Vlasov–Poisson equations based on the asymmetrically-weighted Hermite expansion in velocity space," J. Comput. Phys. **488**, 112252 (2023).
[34]M. Bessemoulin-Chatard and F. Filbet, "On the convergence of discontinuous Galerkin/Hermite spectral methods for the Vlasov–Poisson system," SIAM J. Numer. Anal. **61**(4), 1664–1688 (2023).
[35]T. H. Stix, *The Theory of Plasma Waves, the Theory of Plasma Waves* (McGraw-Hill, New York, 1962).
[36]J. Byers and M. Grewal, "Perpendicularly propagating plasma cyclotron instabilities simulated with a one-dimensional computer model," Phys. Fluids **13**(7), 1819–1830 (1970).
[37]M. Kotschenreuther, "Numerical simulation," Bull. Am. Phys. Soc **34**, 2107–2108 (1988).
[38]A. Dimits and W. W. Lee, "Partially linearized algorithms in gyrokinetic particle simulation," J. Comput. Phys. **107**(2), 309–323 (1993).
[39]A. Y. Aydemir, "A unified Monte Carlo interpretation of particle simulations and applications to non-neutral plasmas," Phys. Plasmas **1**(4), 822–831 (1994).
[40]P. H. Yoon, R. Gaelzer, T. Umeda, Y. Omura, and H. Matsumoto, "Harmonic Langmuir waves. I. Nonlinear dispersion relation," Phys. Plasmas **10**(2), 364–372 (2003).
[41]S. Brunner, E. Valeo, and J. A. Krommes, "Collisional delta-f scheme with evolving background for transport time scale simulations," Phys. Plasmas **6**(12), 4504–4521 (1999).
[42]S. Allfrey and R. Hatzky, "A revised δf algorithm for nonlinear PIC simulation," Comput. Phys. Commun. **154**(2), 98–104 (2003).
[43]M. Campos Pinto, M. Pelz, and P.-H. Tournier, "A δf PIC method with forward-backward Lagrangian reconstructions," Phys. Plasmas **30**(3), 033902 (2023).
[44]V. Roytershteyn and G. L. Delzanno, "Spectral approach to plasma kinetic simulations based on Hermite decomposition in the velocity space," Front. Astron. Space Sci. **5**, 27 (2018).
[45]A. Crestetto, N. Crouseilles, G. Dimarco, and M. Lemou, "Asymptotically complexity diminishing schemes (ACDS) for kinetic equations in the diffusive scaling," J. Comput. Phys. **394**, 243–262 (2019).
[46]V. Kolobov and R. Arslanbekov, "Towards adaptive kinetic-fluid simulations of weakly ionized plasmas," J. Comput. Phys. **231**(3), 839–869 (2012).
[47]L. K. Daldorff, G. Tóth, T. I. Gombosi, G. Lapenta, J. Amaya, S. Markidis, and J. U. Brackbill, "Two-way coupling of a global Hall magnetohydrodynamics model with a local implicit particle-in-cell model," J. Comput. Phys. **268**, 236–254 (2014).
[48]S. Markidis, P. Henri, G. Lapenta, K. Rönnmark, M. Hamrin, Z. Meliani, and E. Laure, "The fluid-kinetic particle-in-cell method for plasma simulations," J. Comput. Phys. **271**, 415–429 (2014).
[49]O. Koshkarov, G. Manzini, G. Delzanno, C. Pagliantini, and V. Roytershteyn, "The multi-dimensional Hermite-discontinuous Galerkin method for the Vlasov–Maxwell equations," Comput. Phys. Commun. **264**, 107866 (2021).